A Novel Platform for Evaluating Dose Rate Effects on Oxidative Damage to Peptides: Toward a High-Throughput Method to Characterize the Mechanisms Underlying the FLASH Effect

Sayan Gupta,[a,1] Jamie L. Inman,[b,1] Jared De Chant,[c] Lieselotte Obst-Huebl,[c] Kei Nakamura,[c] Shawn M. Costello,[d] Susan Marqusee,[e] Jian-Hua Mao,[b] Louis Kunz,[f] Ryan Paisley,[f] Marie-Catherine Vozenin,[f] Antoine M. Snijders,[b,2] Corie Y. Ralston[a,2]

[a] Molecular Biophysics and Integrated Bioimaging Division, [b] Biological Systems and Engineering Division, [c] Accelerator Technology and Applied Physics Division, Lawrence Berkeley National Laboratory, 1 Cyclotron Road, Berkeley, California 94720; [d] Biophysics Graduate Program,

[e] Department of Molecular and Cell Biology, Department of Chemistry; California Institute for Quantitative Biosciences, University of California, Berkeley, California; Chan Zuckerberg Biohub, San Francisco, California; [f] University Hospital and University of Lausanne, Lausanne, Switzerland

Gupta S, Inman J, De Chant J, Obst-Huebl L, Nakamura K, Costello SM, Marqusee S, Mao J.H, Kunz L, Paisley R, Vozenin M-C, Snijders AM, Ralston CY. A Novel Platform for Evaluating Dose Rate Effects on Oxidative Damage to Peptides: Toward a High-Throughput Method to Characterize the Mechanisms Underlying the FLASH Effect. Radiat Res. 200, 000–000 (2023).

High dose rate radiation has gained considerable interest recently as a possible avenue for increasing the therapeutic window in cancer radiation treatment. The sparing of healthy tissue at high dose rates relative to conventional dose rates, while maintaining tumor control, has been termed the FLASH effect. Although the effect has been validated in animal models using multiple radiation sources, it is not yet well understood. Here, we demonstrate a new experimental platform for quantifying oxidative damage to protein sidechains in solution as a function of radiation dose rate and oxygen availability using liquid chromatography mass spectrometry. Using this reductionist approach, we show that for both X-ray and electron sources, isolated peptides in solution are oxidatively modified to different extents as a function of both dose rate and oxygen availability. Our method provides an experimental platform for exploring the parameter space of the dose rate effect on oxidative changes to proteins in solution.

INTRODUCTION

Radiotherapy is currently the standard of care for more than half of all cancer patients (*1*, *2*). Radiotherapy technology has steadily improved over the last several decades with increased beam energy and precision targeting that enable higher doses to be delivered to the tumor while at the same time minimizing dose delivered to surrounding normal tissues. More recently, evidence for beneficial differential effects on tumors versus normal tissues using the delivery of radiation at extremely high dose rates, termed the "FLASH radiotherapy effect," has been revisited after earlier promising studies using microorganisms, cell lines and animal models (*3*–*7*). While the FLASH effect has now been successfully demonstrated in mice (*8*, *9*), mini-pigs and cats (*10*) it has not yet been validated in humans, though trials are currently ongoing (*11*–*14*).

The mechanism of the FLASH effect is complex and likely involves multiple factors encompassing biochemical, cellular and organismal radiation responses including radiolytic oxygen consumption, radical-radical recombination (*15*, *16*), and inflammatory and immunological effects (*17*). Reductionist approaches can be used to isolate the relative contributions of each of these mechanisms, explore at a fundamental level the parameter space in which the FLASH effect operates, and provide a high throughput methodology to probe the FLASH effect. To explore the dynamic kinetics of the FLASH effect, we applied the technique of X-ray footprinting mass spectrometry (XFMS) to determine the relative levels of radiation mediated peptide oxidation as a function of dose rate and oxygen concentration. XFMS is a structural biology method which uses protein oxidation as a means to evaluate protein structure, interactions, and dynamics in solution, and has been used to characterize proteins ranging in size from single small domains to MDa complexes (*18*–*20*), and RNA folding and DNA-protein interactions (*21*, *22*). The method takes advantage of hydroxyl radical creation in aqueous buffers after ionizing irradiation. Hydroxyl radicals are one of the most reactive of species created by irradiation of water, and form permanent modifications on protein side chains, which can then be quantified using standard bottom-up liquid chromatography mass spectrometry (LC-MS) (*23*). While the method is most often used to gain information

[1] These authors contributed equally to the work and are co-first authors.
[2] Correspondence e-mail: cyralston@lbl.gov and amsnijders@lbl.gov.

on protein structure by comparing regions of oxidation as a function of solvent accessibility, here we present its novel use to quantify oxidative damage to short peptides under different FLASH and conventional (CONV) radiation regimes and as a function of oxygen availability.

MATERIALS AND METHODS

Peptides

All samples were prepared at room temperature (20–22°C) and near sea-level (1 atmosphere). The short peptide FKRIVQRIKDFLR was purchased from AnaSpec in lyophilized form at >95% purity, and dissolved in MilliQ water to 10 μM concentration. The pH of the sample after peptide addition was pH 5. Dissolved oxygen levels were measured using a Pyroscience Firesting OXF50 handheld O_2 meter. Oxygen levels in samples before preparation with N_2 gas were 21–22%, indicating full air saturation. Low-oxygen samples were further prepared by bubbling N_2 gas through samples for one min and then cycling into a nitrogen environment in a Coy Anaerobic Chamber. Oxygen levels were then measured in the anaerobic chamber prior to triple-bagging samples in plastic bags with zip closures for transport to either the synchrotron X-ray beamline or the XRAD X-ray instrument, as previously described (*24*). Before transport, O_2 levels in the low-oxygen samples measured 1–3%. After each irradiation set, a water sample was irradiated using the same sample procedure, and immediately measured for dissolved O_2 level. Low-oxygen samples measured 4–6% O_2 level, indicating that low-oxygen conditions were maintained throughout the irradiation procedure.

For the synchrotron FLASH X-ray irradiation, samples were delivered through the X-ray beam using a syringe pump as described below. For CONV X-ray irradiation in the XRAD instrument, and for electron irradiation at the LINAC, peptide samples were aliquoted into 1.5 mL Eppendorf tubes using a volume of 100 μL. In all cases, samples were frozen immediately after irradiation.

Irradiations and Dosimetry

Advanced Light Source Synchrotron Beamline 3.3.1. The Advanced Light Source (ALS) beamline 3.3.1 delivers a broadband X-ray beam with critical energy 3.1 keV from a 1.3T bending magnet and is additionally focused with a Pt-coated X-ray mirror to a minimum beam size of 80–100 (H) μm. For all exposures, an X-ray slit was used to further define the beam and reduce scattering. Samples were prepared in syringes either on the bench or in an anaerobic chamber, and placed in the endstation syringe pump to deliver via liquid jet through the X-ray beam at various speeds as previously described (*25*). For a 2.5 mL syringe, a jet nozzle of 75 μm, a jet speed of 20 m/s, and slit size of 1.8 mm, samples were exposed to X rays for 90 μs, whereas with a jet speed of 4 m/s, samples were exposed for 450 μs. Aluminum attenuation was further used to achieve desired doses of 1.6, 3, 4.2, 8.2, 15 and 21 Gy, with dose rates ranging from 17 to 47 kGy/s. T1 (Table 1). Sample volume collected was 100 μL. In all cases the ALS ring current was 500 mA.

Dosimetry was performed using calibrated Gafchromic HDv2 radiochromic films (RCF). The active layer of the RCF is sensitive to ionizing radiation and undergoes a change in color which can be directly related to the dose that would be absorbed by a sample in that environment. The films were placed at the focal position of the X-ray beam in place of the liquid jet and irradiated the day prior to sample irradiation. The films were irradiated with various exposure times and with varying levels of attenuation, resulting in doses applied to the film in the range of 1.4–8.4 kGy, to characterize the dose rate profile of the beamline. A Uniblitz XRS6 X-ray shutter (Vincent Associates, NY) was used to control the exposure time.

An EPSON Expression 12000XL scanner was utilized to scan the films in landscape format, with all image correction features turned off, at a resolution of 600 dpi (42.3 μm/pixel) in transmission mode. The scanned images were saved as 16-bit grayscale TIFF files. Scanning was conducted several days after irradiation to allow for stabilization of the optical density development after irradiation. Each scan was calibrated using a NIST-calibrated transparent step wedge. This calibration process involves converting the raw data to optical density (OD), which can be directly correlated to the measured dose. The conversion from OD to dose was done according to the high dose rate calibration of Gafchromic films (*26*).

TABLE 1
Exposure Times, Attenuation, Doses and Dose Rates for Irradiation Using Synchrotron Beamline 3.3.1 with Jet Sample Delivery

Exposure (μs)	Al thickness (inches)	Dose (Gy)	Dose rate (kGy/s)
90	0.012	1.6	18
90	0.010	3.0	34
90	0.009	4.2	47
450	0.012	8.2	18
450	0.010	15	34
450	0.009	21	47

Notes. In all cases slit width was 1.8 mm, and ALS ring current was 500 mA. The dosimetry based on Gafchromic film measurements comes with a measurement uncertainty of ±5.7%.

The X-ray intensity was not spatially uniform vertically, which resulted in a variable dose rate as the jet passed through the beam. The dose measured in each pixel in an RCF scan was divided by the exposure time of the RCF to calculate the dose rate measured in each pixel. The profile was then scaled by the exposure time per pixel of the liquid jet at the two speeds (4 and 20 m/s). The exposure time per pixel is the pixel width (42.3 μm) divided by the jet speed and represents the time the sample would be irradiated as it passes through the space that pixel represents. By then integrating the dose profile vertically, the non-uniformity of the X-ray intensity was taken into account, for the derivation of the radiation dose and dose rate received by the liquid jet.

There was also some slight non-uniformity in the horizontal X-ray intensity across the width of the water jet (75 μm). Due to the limited resolution of the RCF scans at that scale, the dose values reported here were calculated by fitting the integrated dose profile to a double Gaussian and then averaging over the width of the water jet (75 μm). A double Gaussian fit was chosen as the focal spot of the X-ray beam is composed of the X-ray mirror bending the two wings of the synchrotron radiation over each other. An example of this analysis and the endstation configuration is shown in Figure 2.

XRAD320 irradiation

CONV dose rate X-ray irradiations were performed at Lawrence Berkeley National Laboratory (LBNL) using the 320-kVp XRAD320 X-ray machine (Precision X-ray, CT, USA), operated at 300 kVp, 10mA. A 0.5mm Cu beam hardening filter was in place during irradiations. Peptide samples were irradiated on a rotating platform with dose rates 0.017-0.020 Gy/s, varying exposure time to attain doses of 0.5, 0.7, 1.1, 2.8, 14.9 or 14.6 Gy (Table 2). Note that one additional T2 exposure using 2 mA and longer exposure time was also taken to attain 15 Gy exposure for comparison at a lower dose rate of 0.004 Gy/s. All peptides were arranged on the rotating platform in a circle pattern such that all samples were equidistant from the center of the platform. Dosimetry was performed using a RadCal dosimeter (Radcal 10X6-0.18 ion chamber) and a single point ion chamber measurement was taken in the middle of the platform to verify dose.

Electron irradiation

For electron irradiation at both CONV and FLASH dose rates, peptide samples were irradiated at the Oriatron eRT6 linear accelerator delivering a 6 MeV pulsed electron beam, and located at the University of Lausanne, Lausanne, Switzerland. Doses were 5, 10, and 15 Gy, with three target dose rates of 0.1, 100, and 10^6 Gy/s. (Table 3) T3

TABLE 2
Exposure Times, Voltage, Doses and Dose Rates for Irradiation Using XRAD

Voltage (kV), current (mA)	Time (s)	Dose (Gy)	Dose rate (Gy/s)
300, 10	29	0.5	0.017
300, 10	38	0.7	0.018
300, 10	61	1.1	0.018
300, 10	139	2.8	0.020
300, 10	739	14.9	0.020
300, 2	3,561	14.6	0.0041

Note. The dosimetry based on a RadCal dosimeter comes with a measurement uncertainty of ±4%.

Dosimetry at the sample position was performed using Gafchromic films, an Advanced Markus chamber, and ACCT (*27*, *28*).

Liquid chromatography mass spectrometry (LC-MS) and data analysis

Irradiated samples were injected at a flow rate of 100 μL/min onto a 150 mm ThermoFisher PepMap 100 C18 HPLC column with 2 μm particle size and diameter of 1 mm. Protein was then eluted with a gradient of 10–65% buffer B (90% Acetonitrile, 0.1% Formic Acid) at a flow rate of 20 mL/min over 5 min, and then of 65-99% buffer B over 6 s, and then held at 99% buffer B for 3 min prior to a washing step and equilibration at 10% buffer B. Protein was eluted directly into a Q Exactive Orbitrap Mass Spectrometer operating in positive mode (resolution 140,000, AGC target 1e6, maximum IT 50 ms, scan range 200–2,000 m/z).

Peptide analysis was performed using the Byos® (Protein Metrics Inc) integrated software platform. Byos encompasses the Byonic™ MS/MS search engine and the Byologic® peptide analysis software. The Byos oxidative footprinting workflow automatically extracts ion chromatograms and reports the quantification of modifications relative to the unmodified peptide based on the extracted ion chromatograms. Peptide-level analysis was reported as a percent modification of the oxidized peptide relative to the native peptide. Mass shifts of +16 Da at the peptide level were specifically quantified. For higher doses, low levels of the +32 Da oxidation were observed in some samples at an order of magnitude lower level than the +16 Da. A complete analysis of +32 Da and other lower level oxidative products would require higher doses and is outside the scope of this paper. After peptide level analysis, results are exported to Excel, and percent modification is plotted as a function of dose.

RESULTS

Dose Rate Effects on Peptide Damage

When biological samples are irradiated, the radiolysis of water generates free radicals which can, in turn, damage proteins, lipids and DNA leading to cellular dysfunction or cell death. We used a short peptide (sequence FKRIVQRIKDFLR) as an in vitro experimental model to study the effect of FLASH and CONV radiation dose rates on hydroxyl radical mediated protein damage, using X-ray and electron radiation (Fig. 1). This peptide was chosen because it contains several residues reactive to hydroxyl radicals, but does not contain cysteine and methionine, which are highly sensitive to handling, producing oxidations even in the absence of radiation. X-ray FLASH irradiation was performed at the Advanced Light Source beamline 3.3.1 where samples passed through the X-ray beam using a sample jet and prescribed doses were delivered to individual samples by adjusting the jet speed and placing aluminum attenuators in the beam path (Fig. 2 and Table 1). CONV X-ray doses were delivered using a cabinet X-ray machine operated at 300 kVp and 10 mA (Table 2).

Our analysis focused on the oxidative modification of amino acids as measured by a +16 Da shift in the LC-MS profile and the cumulative percent modification across the peptide as a function of delivered dose. For both X-ray and electron irradiation, we observed an approximately linear increase in damage with increasing radiation dose at both FLASH and CONV dose rates (Figs. 3 and 4). All data was fit with a linear function, though further work would have to be conducted to determine whether there is a saturation effect with higher doses and/or higher dose rates. For both X-ray and electron irradiation, we also observed higher peptide oxidative damage with low (CONV) vs. high (FLASH) dose rates. X-ray dose rates varied from 0.2 Gy/s for CONV irradiation to 18 to 47 kGy/s for FLASH dose rate irradiation, while for electron irradiation, target dose rates were 0.1, 100, and 10^6 Gy/s (Table 3). In both cases, CONV irradiation dose rates resulted in a 1.5–2.9 fold increase in modification over

TABLE 3
Parameters for Electron Irradiations

Dose (Gy)	Film dose (Gy)	SSE (mm)	No. pulses	Pulse width (μs)	Freq (Hz)	Dose per pulse (Gy)	Beam on time (ms)	Mean dose rate (Gy/s)	Instant-aneous dose rate (Gy/s)
5	4.7	960	5	1.8	100	1	40	125	5.56×10^5
10	9.6	960	10	1.8	100	1	90	111	5.56×10^5
15	14.5	960	15	1.8	100	1	140	107	5.56×10^5
5	5.2	455	1	1.8	100	5	1.8×10^{-3}	2.77×10^6	2.77×10^6
10	10.5	330	1	1.8	100	10	1.8×10^{-3}	5.56×10^6	5.56×10^6
15	15.7	271	1	1.8	100	15	1.8×10^{-3}	8.33×10^6	8.33×10^6
5	5.1	600	285	1	10	0.017	28,500	0.17	1.7×10^4
10	10.2	600	570	1	10	0.017	57,000	0.17	1.7×10^4
15	15.2	600	850	1	10	0.017	85,000	0.17	1.7×10^4

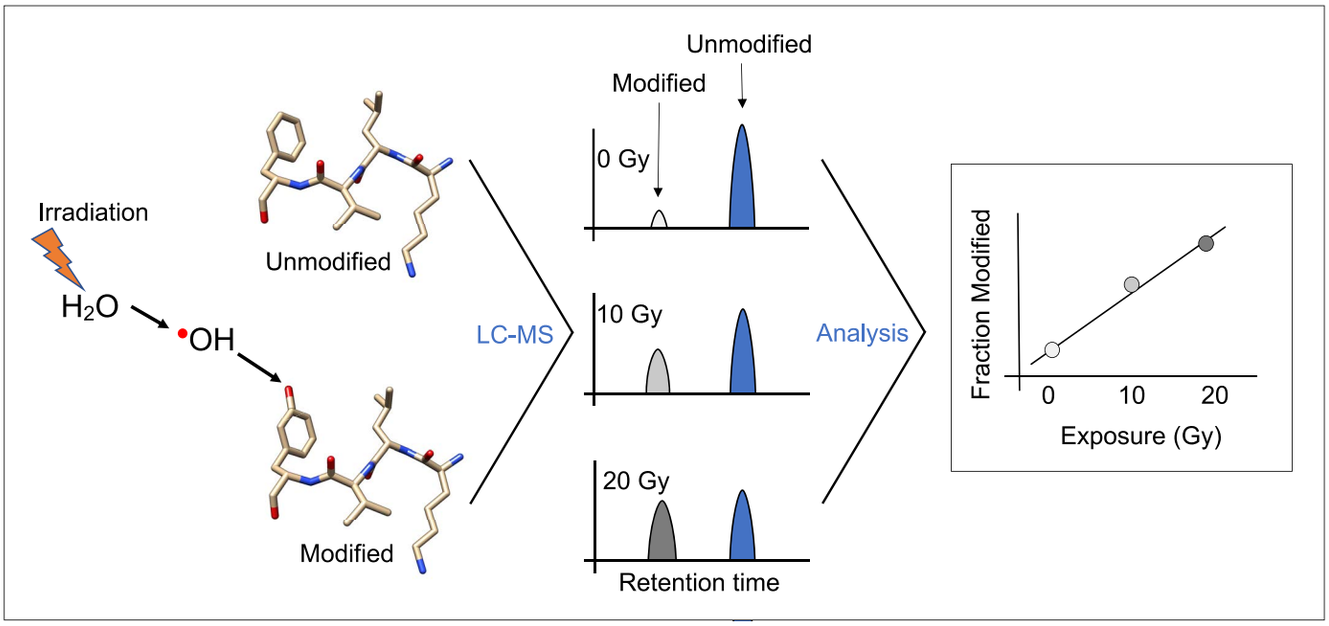

FIG. 1. Overview of concept. Radiolysis of water results in radical species, including hydroxyl radicals and electrons. Hydroxyl radicals are very reactive to protein, and will modify sidechains covalently, often resulting in an OH moiety addition to aromatic rings and methionine. Modifications are detected using LC-MS. The fraction of molecules modified is calculated using the area under the extracted ion chromatograms for the native and modified peptides, and plotted as a function of dose.

the FLASH dose rates, as measured by the slope of the linear fit to the data (Table 4).

Peptide Oxidative Damage is Oxygen Dependent

To determine if the oxidative peptide damage was dependent on ambient oxygen levels, we compared peptide damage under ambient (21% O_2) vs. reduced oxygen (4–6% O_2) conditions using CONV and FLASH X-ray irradiation (Fig. 5). For both CONV and FLASH irradiation, we observed a 2.2-fold decrease in oxidative damage under reduced oxygen conditions, as measured by the slope of the linear fit to the data (Table 4). These results confirm that oxygen is critical in the peptide damage pathway.

DISCUSSION

Hydroxyl radical oxidative damage to proteins has a long history of use in structural biology as a characterization method for protein structure and dynamics, and in combination with mass spectrometry methods is largely referred to as hydroxyl radical protein footprinting (*23*, *29*, *30*). When X-ray sources are used, the method is termed X-ray Footprinting Mass Spectrometry (XFMS) (*31*). Because hydroxyl radical footprinting is a mature field, the mechanisms and quantification of oxidative modifications to dilute proteins in solution by hydroxyl radical is well understood. With this method, radiolysis of water or chemical methods are used to generate hydroxyl radicals in solution, which then oxidatively modify protein/peptide sidechains. Subsequent LC-MS analysis is used to determine the location of oxidative changes, which provides a map of solvent accessibility and is used to infer structural information about the protein/peptide in solution. Many radical species are produced upon radiolysis of water, including hydroperoxyl, superoxide, and hydroxyl radicals, and these radicals re-combine on the sub-microsecond timescale to produce further species, which react with protein side chains and backbone with varying rate constants, as has been reviewed elsewhere (*32–35*). In particular, the reaction rate of the hydroxyl radical with protein amino acids can be at least an order of magnitude higher than the reaction rate of other species such as hydrogen peroxide or solvated electrons with amino acids (*23*), and so with the XFMS method, oxidative modification upon radiolysis of dilute aqueous protein or peptide solutions is expected to be largely due to hydroxyl radical mediated reactions.

Here, we have leveraged this accumulated knowledge to apply XFMS to the characterization of the dose rate dependent oxidation of dilute peptides in solution under both aerobic and anaerobic conditions. We used dilute peptides in water to maintain and measure indirect radiation damage; a concentration of 10 micromolar peptide in 55 M water ensured that X-ray or electron interactions were mainly limited to water molecules rather than peptide molecules. In addition, we did not include radical scavengers to focus directly on the reaction of hydroxyl radicals with protein residues.

The +16 Da oxidative modification on protein sidechains is the most common oxidative product observed in the XFMS method. For amino acids in solution, reactivities of sidechains with hydroxyl radical are highest for Cys, Trp, Tyr and Met, with rates $\sim 10^{10}$ M^{-1} s^{-1}, while reactivities

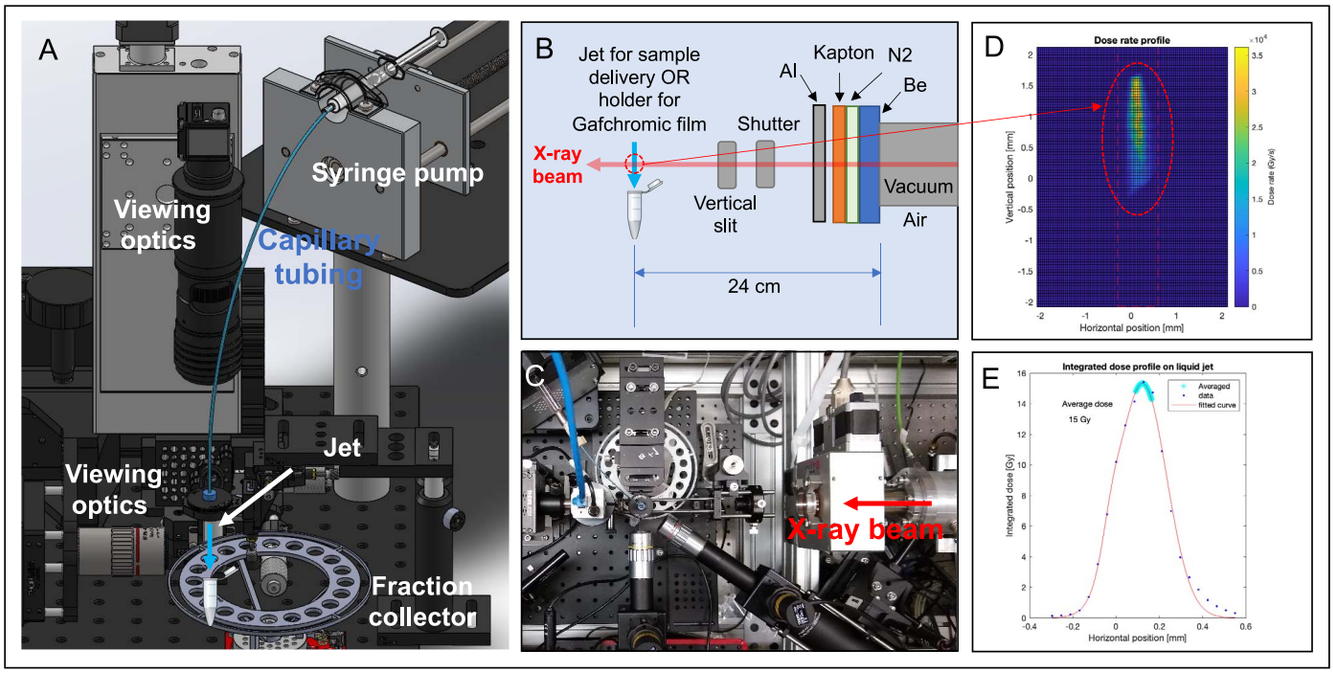

FIG. 2. Sample delivery setup and dosimetry estimation at the ALS beamline 3.3.1 beamline. Panel A: CAD model of the syringe pump, optics, jet, and fraction collector. Sample is delivered in a stream of liquid from a jet nozzle; as it travels from the nozzle to the fraction collector, it passes through the X-ray beam and the speed of the liquid determines the exposure time. Panel B: Overview of the components used in the dose estimation. Panel C: Closeup of jet and fraction collector in the endstation. Panel D: Example of RCF film exposure at position of the jet (normalized to the dose rate). Panel E: Dose profile of the X-ray beam measured by an RCF (scaled to water-jet exposure time). The vertically integrated dose is fit to a double Gaussian and an average over 75 μm of the peak of the fit is reported as the dose absorbed by the sample present in the liquid jet.

with the amino acids Phe, His, Arg, Ile, and Leu are lower at $\sim 10^9$ M^{-1} s^{-1}, and decrease to 10^7 M^{-1} s^{-1} with Gly (*23*). Reactivities of residues within proteins will change with the local environment and may not necessarily follow this pattern of reactivity, and we note in our studies that for a given +16 Da addition, we did not determine which residue was modified, only that the peptide overall showed a +16 Da modification as measured by mass shift. Less common modifications seen in the XFMS experiment are +32 Da (addition of two OH moieties and loss of two H), +48

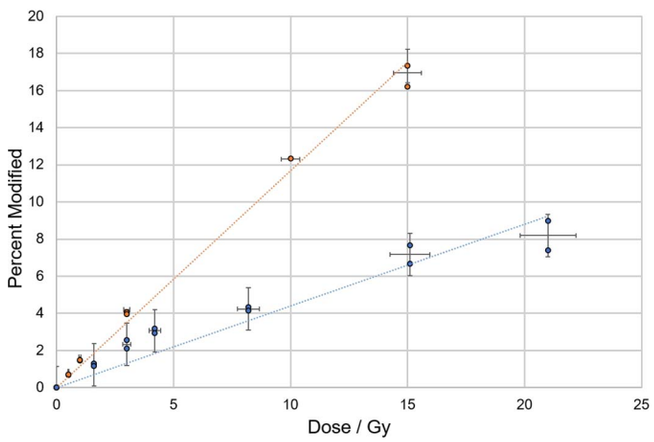

FIG. 3. Comparison of FLASH vs. CONV X-ray irradiation. Comparison between oxidation of the FKRIVQRIKDFLR peptide on the XRAD instrument with conventional dose rate of ∼0.02 Gy/s (orange) and the synchrotron beamline with FLASH dose rates of $\sim 10^4$ Gy/s (blue), for air-saturated samples (21–22% O_2). Actual dose rates are shown in Tables 1 and 2. Dotted lines are linear fits to the average of each set. Error bars indicate standard deviation across replicate measurements.

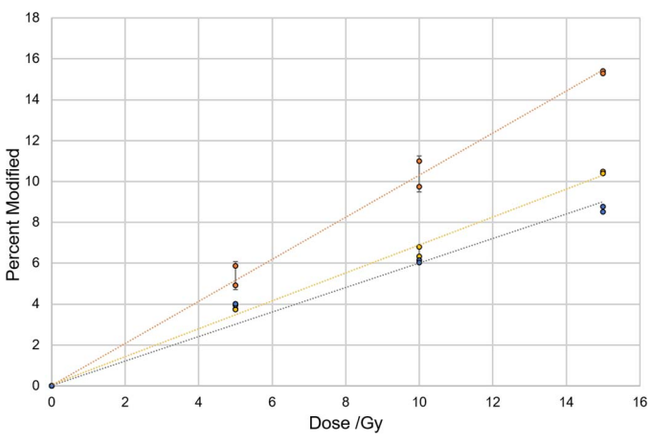

FIG. 4. Comparison between oxidation of the FKRIVQRIKDFLR peptide using electron irradiation at targeted dose rates of 0.1 Gy/s (orange), 100 Gy/s (yellow) and 10^6 Gy/s (blue), for air-saturated samples (21–22% O_2). Actual dose rates for each applied dose are shown in Table 3. Dotted lines are linear fits to the average of each set. Error bars indicate standard deviation across replicate measurements.

TABLE 4

Values of Linear Fits to Average Percent Modification, with Corresponding Coefficient of Determination (R^2)

Experiment	Fig. (s)	Slope of linear fit to average of data (% modification/dose in Gy)	R^2 value
FLASH dose rate X-ray irradiation (Table 1) under air-saturated conditions	3 and 5 (bottom panel)	0.44	0.9166
FLASH dose rate X-ray irradiation (Table 1) under low-oxygen conditions	5 (bottom panel)	0.20	0.9943
CONV dose rate X-ray irradiation (Table 2) under air-saturated conditions	3 and 5 (top panel)	1.27	0.9538
CONV dose rate X-ray irradiation (Table 2) under low-oxygen conditions	5 (top panel)	0.59	0.9959
Electron irradiation at targeted dose rate of 0.1 Gy/s (Table 3) under air-saturated conditions	4	1.03	0.9728
Electron irradiation at targeted dose rate of 100 Gy/s (Table 3) under air-saturated conditions	4	0.69	0.9964
Electron irradiation at targeted dose rate of 10^6 Gy/s (Table 3) under air-saturated conditions	4	0.60	0.9994

Da (addition of three OH moieties and loss of 3 H), +14 Da (addition of O and loss of 2 H), and -30 Da (loss of COO and gain of O).

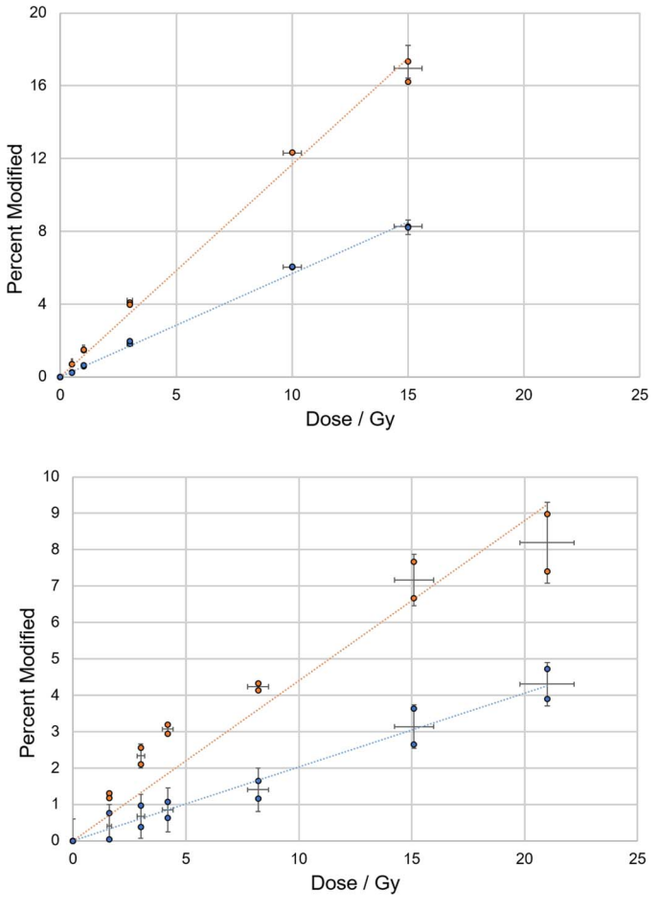

FIG. 5. Effect of O2 availability. Comparison between oxidative modification rates of the FKRIVQRIKDFLR peptide for air-saturated (21–22% O_2) (orange) and low-oxygen (blue) buffer. Top panel: XRAD instrument with conventional dose rate irradiation of ~0.02 Gy/s. Bottom panel: Synchrotron beamline with FLASH dose rate irradiation of $\sim 10^4$ Gy/s (blue). Actual dose rates for each dose are shown in Tables 1 and 2. Dotted lines are linear fits to the average of each set. Error bars indicate standard deviation across replicate measurements.

Overall, our results show an increasing level of the +16 Da modification product as a function of dose. Electron and X-ray irradiation have fundamental differences in absorption profiles and linear energy transfer (*36*, *37*), and conventional X-ray machines have different energy profiles than synchrotron X-ray beamlines. Despite these differences, the results here comparing CONV and FLASH dose rates for both X-ray and electron irradiation are consistent with radiochemical results observed with the FLASH dose rate effect, in which lower dose rates can result in more peptide damage. Further, the oxidative damage when comparing fully aerated to low-oxygen samples demonstrated that the presence of dissolved oxygen significantly affects the amount of oxidative damage incurred by the peptides in solution. Previous XFMS studies of proteins in an anaerobic environment have also shown that oxidative damage is reduced when dissolved oxygen in solution is lowered (*24*), since the mechanism of oxidative damage in the form of OH moiety addition (and other products) generally relies on the presence of oxygen. One explanation for the reduced damage of peptides in water using high dose rate irradiation is based upon the "oxygen depletion effect" (*38–40*), in which oxygen is consumed quickly by reactions under the high dose rate irradiation, and exposure times are short enough that sufficient oxygen for further reactions does not diffuse back into solution. However, recent measurements refute the oxygen depletion hypothesis at high dose rate at doses around 10 Gy (*36*, *41*) while at the same time the production of reactive oxygen species has been shown to be reduced (*42*, *43*). Our results demonstrate the effect of oxygen availability on hydroxyl radical mediated oxidative damage to protein sidechains in solution; even with no scavengers or competing cellular processes present, the availability of oxygen determines the extent to which sidechains are oxidatively modified for both CONV and FLASH dose rates. In addition, the higher dose rates resulted in less oxidative damage, suggesting that the early kinetics of reactions might be altered by recombination and/or diffusion processes. With this reductionist approach, it will be possible to thoroughly quantify the extent of damage as a function of oxygen level and peptide

concentration, as a function of a wide range of dose rates, and as cellular components and radical scavengers are added to the sample environment. In addition, MS/MS approaches can be used to quantify and localize oxidative damage to specific to amino acid residues in peptides or proteins.

ACKNOWLEDGMENTS

This work was partially conducted at the Advanced Light Source and the Molecular Foundry, which are supported by the Office of Science of the U.S. Department of Energy (DOE) under contract DE-AC02-05CH11231. Work was supported by the NIH R01 GM126218 and NIH P30 GM124169, the IARPA Interagency Agreement IARPA-20008-D2021-2107310008, and Laboratory Directed Research and Development funding under U.S. Department of Energy Contract No. DE-AC02-05CH11231. SM is a Chan Zuckerberg Biohub investigator. Additionally, funding was provided by Swiss National Science Foundation grant MAGIC - FNS CRS II5_186369 (to MCV and supporting RP) and National Institutes of Health grant P01CA244091-01 (to MCV).

Received: July 6, 2023; accepted: October 5, 2023; published online: Month 00, 2023

REFERENCES

1. Begg AC, Stewart FA, Vens C. Strategies to improve radiotherapy with targeted drugs. Nat Rev Cancer. 2011; 11 (4):239-53.
2. Delaney G, Jacob S, Featherstone C, Barton M. The role of radiotherapy in cancer treatment: estimating optimal utilization from a review of evidence-based clinical guidelines. Cancer. 2005; 104 (6):1129-37.
3. Dewey DL, Boag JW. Modification of the oxygen effect when bacteria are given large pulses of radiation. Nature. 1959; 183 (4673):1450-1.
4. Hornsey S, Bewley DK. Hypoxia in mouse intestine induced by electron irradiation at high dose-rates. Int J Radiat Biol Relat Stud Phys Chem Med. 1971; 19 (5):479-83.
5. Town CD. Radiobiology. Effect of high dose rates on survival of mammalian cells. Nature. 1967; 215 (5103):847-8.
6. Ling CC, Michaels HB, Epp ER, Peterson EC. Oxygen diffusion into mammalian cells following ultrahigh dose rate irradiation and lifetime estimates of oxygen-sensitive species. Radiat Res. 1978; 76 (3):522-32.
7. Field SB, Bewley DK. Effects of dose-rate on the radiation response of rat skin. Int J Radiat Biol Relat Stud Phys Chem Med. 1974; 26 (3):259-67.
8. Favaudon V, Caplier L, Monceau V, Pouzoulet F, Sayarath M, Fouillade C, et al. Ultrahigh dose-rate FLASH irradiation increases the differential response between normal and tumor tissue in mice. Sci Transl Med. 2014; 6 (245):245ra93.
9. Montay-Gruel P, Petersson K, Jaccard M, Boivin G, Germond JF, Petit B, et al. Irradiation in a flash: Unique sparing of memory in mice after whole brain irradiation with dose rates above 100Gy/s. Radiother Oncol. 2017; 124 (3):365-9.
10. Vozenin MC, De Fornel P, Petersson K, Favaudon V, Jaccard M, Germond JF, et al. The Advantage of FLASH Radiotherapy Confirmed in Mini-pig and Cat-cancer Patients. Clin Cancer Res. 2019; 25 (1):35-42.
11. Bourhis J, Sozzi WJ, Jorge PG, Gaide O, Bailat C, Duclos F, et al. Treatment of a first patient with FLASH-radiotherapy. Radiother Oncol. 2019; 139:18-22.
12. Mascia AE, Daugherty EC, Zhang Y, Lee E, Xiao Z, Sertorio M, et al. Proton FLASH Radiotherapy for the Treatment of Symptomatic Bone Metastases: The FAST-01 Nonrandomized Trial. JAMA Oncol. 2023; 9 (1):62-9.
13. Gaide O, Herrera F, Jeanneret Sozzi W, Goncalves Jorge P, Kinj R, Bailat C, et al. Comparison of ultra-high versus conventional dose rate radiotherapy in a patient with cutaneous lymphoma. Radiother Oncol. 2022; 174:87-91.
14. van Marlen P, van de Water S, Dahele M, Slotman BJ, Verbakel W. Single Ultra-High Dose Rate Proton Transmission Beam for Whole Breast FLASH-Irradiation: Quantification of FLASH-Dose and Relation with Beam Parameters. Cancers (Basel). 2023; 15 (9).
15. Abolfath R, Grosshans D, Mohan R. Oxygen depletion in FLASH ultra-high-dose-rate radiotherapy: A molecular dynamics simulation. Med Phys. 2020; 47 (12):6551-61.
16. Labarbe R, Hotoiu L, Barbier J, Favaudon V. A physicochemical model of reaction kinetics supports peroxyl radical recombination as the main determinant of the FLASH effect. Radiother Oncol. 2020; 153:303-10.
17. Jin JY, Gu A, Wang W, Oleinick NL, Machtay M, Spring Kong FM. Ultra-high dose rate effect on circulating immune cells: A potential mechanism for FLASH effect? Radiother Oncol. 2020; 149:55-62.
18. Gupta S, Chai J, Cheng J, D'Mello R, Chance MR, Fu D. Visualizing the kinetic power stroke that drives proton-coupled zinc (II) transport. Nature. 2014; 512 (7512):101-4.
19. Deperalta G, Alvarez M, Bechtel C, Dong K, McDonald R, Ling V. Structural analysis of a therapeutic monoclonal antibody dimer by hydroxyl radical footprinting. MAbs. 2013; 5 (1):86-101.
20. Bohon J, Jennings LD, Phillips CM, Licht S, Chance MR. Synchrotron protein footprinting supports substrate translocation by ClpA via ATP-induced movements of the D2 loop. Structure. 2008; 16 (8):1157-65.
21. Gupta S, Cheng H, Mollah AK, Jamison E, Morris S, Chance MR, et al. DNA and protein footprinting analysis of the modulation of DNA binding by the N-terminal domain of the Saccharomyces cerevisiae TATA binding protein. Biochemistry. 2007; 46 (35): 9886-98.
22. Clatterbuck Soper SF, Dator RP, Limbach PA, Woodson SA. In vivo X-ray footprinting of pre-30S ribosomes reveals chaperone-dependent remodeling of late assembly intermediates. Mol Cell. 2013; 52 (4): 506-16.
23. Xu G, Chance MR. Hydroxyl radical-mediated modification of proteins as probes for structural proteomics. Chem Rev. 2007; 107 (8):3514-43.
24. Kristensen LG, Holton JM, Rad B, Chen Y, Petzold CJ, Gupta S, et al. Hydroxyl radical mediated damage of proteins in low oxygen solution investigated using X-ray footprinting mass spectrometry. J Synchrotron Radiat. 2021; 28 (Pt 5):1333-42.
25. Rosi M, Russell B, Kristensen LG, Farquhar ER, Jain R, Abel D, et al. An automated liquid jet for fluorescence dosimetry and microsecond radiolytic labeling of proteins. Commun Biol. 2022; 5 (1):866.
26. Bin JH, Ji Q, Seidl PA, Raftrey D, Steinke S, Persaud A, et al. Absolute calibration of GafChromic film for very high flux laser driven ion beams. Rev Sci Instrum. 2019; 90 (5):053301.
27. Jorge PG, Jaccard M, Petersson K, Gondre M, Duran MT, Desorgher L, et al. Dosimetric and preparation procedures for irradiating biological models with pulsed electron beam at ultra-high dose-rate. Radiother Oncol. 2019; 139:34-9.
28. Goncalves Jorge P, Grilj V, Bourhis J, Vozenin MC, Germond JF, Bochud F, et al. Technical note: Validation of an ultrahigh dose rate pulsed electron beam monitoring system using a current transformer for FLASH preclinical studies. Med Phys. 2022; 49 (3):1831-8.
29. Wang L, Chance MR. Structural mass spectrometry of proteins using hydroxyl radical based protein footprinting. Anal Chem. 2011; 83 (19):7234-41.

30. Liu XR, Rempel DL, Gross ML. Protein higher-order-structure determination by fast photochemical oxidation of proteins and mass spectrometry analysis. Nat Protoc. 2020; 15 (12):3942-70.

31. Gupta S, Celestre R, Petzold CJ, Chance MR, Ralston C. Development of a microsecond X-ray protein footprinting facility at the Advanced Light Source. J Synchrotron Radiat. 2014; 21 (Pt 4): 690-9.

32. Buxton GV. Critical Review of rate constants for reactions of hydrated electrons, hydrogen atoms and hydroxyl radicals (·OH/·O− in Aqueous Solution. Journal of Physical and Chemical Reference Data. 1988; 17 (2):513-886.

33. Garrison WM. Reaction Mechanisms in the Radiolysis of Peptides, Polypeptides, and Proteins. Chem Rev. 1987; 87:381-98.

34. Davies MJ. Protein oxidation and peroxidation. Biochem J. 2016; 473 (7):805-25.

35. Hawkins CL, Davies MJ. Detection, identification, and quantification of oxidative protein modifications. J Biol Chem. 2019; 294 (51):19683-708.

36. Jansen J, Knoll J, Beyreuther E, Pawelke J, Skuza R, Hanley R, et al. Does FLASH deplete oxygen? Experimental evaluation for photons, protons, and carbon ions. Med Phys. 2021; 48 (7):3982-90.

37. Hunter N, Muirhead CR. Review of relative biological effectiveness dependence on linear energy transfer for low-LET radiations. J Radiol Prot. 2009; 29 (1):5-21.

38. Pratx G, Kapp DS. A computational model of radiolytic oxygen depletion during FLASH irradiation and its effect on the oxygen enhancement ratio. Phys Med Biol. 2019; 64 (18):185005.

39. Petersson K, Adrian G, Butterworth K, McMahon SJ. A Quantitative Analysis of the Role of Oxygen Tension in FLASH Radiation Therapy. Int J Radiat Oncol Biol Phys. 2020; 107 (3):539-47.

40. Favaudon V, Labarbe R, Limoli CL. Model studies of the role of oxygen in the FLASH effect. Med Phys. 2022; 49 (3):2068-81.

41. Cao X, Zhang R, Esipova TV, Allu SR, Ashraf R, Rahman M, et al. Quantification of Oxygen Depletion During FLASH Irradiation In Vitro and In Vivo. Int J Radiat Oncol Biol Phys. 2021; 111 (1):240-8.

42. Kacem H, Almeida A, Cherbuin N, Vozenin MC. Understanding the FLASH effect to unravel the potential of ultra-high dose rate irradiation. Int J Radiat Biol. 2022; 98 (3):506-16.

43. Montay-Gruel P, Acharya MM, Petersson K, Alikhani L, Yakkala C, Allen BD, et al. Long-term neurocognitive benefits of FLASH radiotherapy driven by reduced reactive oxygen species. Proc Natl Acad Sci U S A. 2019; 116 (22):10943-51.